A Multi-mode Direct Conversion Receiver for Joint Communication and Radar Sensing

Sandra George
Barkhausen Institut
Dresden, Germany
sandra.george@barkhauseninstitut.org

Padmanava Sen
Barkhausen Institut
Dresden, Germany
padmanava.sen@barkhauseninstitut.org

Corrado Carta
Technische Universität Berlin
IHP Microelectronics GmbH
carta@ihp-microelectronics.com

***Abstract*—This paper presents a reconfigurable direct conversion receiver in $22\,\mathrm{nm}$ FDSOI technology with $25\,\mathrm{GHz}$ center frequency, implemented for Joint Communication and Radar Sensing (JC&S) applications. The receiver employs a multi-mode 2-stage cascaded common source Low Noise Amplifier (LNA) and a multi-mode Gilbert cell down-conversion mixer. The receiver can be switched between radar mode and communication mode delivering more linearity in radar mode and higher gain in communication mode. In the communication mode, the receiver consumes a power of $22.4\,\mathrm{mW}$ while delivering an overall gain of $24.5\,\mathrm{dB}$ and an $\mathrm{iP_{1dB}}$ of $-28\,\mathrm{dBm}$ excluding the baseband buffer. In the radar mode, the receiver consumes a maximum DC power of $11.63\,\mathrm{mW}$ delivering a maximum receiver gain of $14.8\,\mathrm{dB}$ and an $\mathrm{iP_{1dB}}$ of $-20\,\mathrm{dBm}$ at $25\,\mathrm{GHz}$. The receiver consumes an area of $0.74\,\mathrm{mm^2}$ including pads and a core area of $0.15\,\mathrm{mm^2}$.**

***Index Terms*—Direct-Conversion receiver, Joint Communication and radar sensing, FDSOI, millimeter-wave integrated circuits**

I. Introduction

In the recent years, there has been a significant surge in research activities towards integrating communication and sensing technologies. Endorsed also by several industrial leaders, Joint Communication and Sensing (JC&S) has the potential to be one of the key features of future 6G systems [1]. The advantages of JC&S are evident through its different modes that are possible with both functionalities. Apart from the efficient and flexible use of the resources, this technology can bring down the cost, size and power consumption, while simultaneously enhancing the overall performance and safety of the system when co-designed. For an efficient co-designed implementation of such a system, reconfigurability will be a requirement for the key elements including but not limited to the hardware components. By incorporating reconfigurable and programmable circuitry such as radio frequency front-ends, JC&S can be better supported in future communication networks and applications [2].

In this paper, a multi-mode direct conversion receiver comprising of an LNA and down-converion mixer tunable with respect to frequency, gain and linearity is presented. Typically, radar receivers require higher linearity to detect close targets without being saturated, while the communication receiver requires very high gain to mitigate the path loss the signal endures. For a half-duplex JC&S receiver, the receiver can operate in a high gain-low linearity communication mode and a low gain-high linearity radar mode.

This design was implemented in $22\,\mathrm{nm}$ Fully Depleted Silicon On Insulator (FDSOI) which offers high performance mm-Wave devices with very high $\mathrm{f_T}$ and $\mathrm{f_{max}}$. The reported $\mathrm{f_T}$ and $\mathrm{f_{max}}$ in this technology referenced to the the top metal layer is $240\,\mathrm{GHz}$ and $230\,\mathrm{GHz}$ respectively [3]. This makes the technology a very good candidate for RF front-end integration in the 5G NR band and the future mm-Wave bands. This technology allows the use of vertical gates and higher gate pitch (2x & 3x) that reduces the gate resistance and allows the transistors to be placed closer to each other. Super-low threshold voltage (slvt) transistors with 2x gate pitch and vertical gates were used for the design of the LNA and mixer core.

This work proposes a $25\,\mathrm{GHz}$ multi-mode direct conversion mixer with a maximum gain of $24.5\,\mathrm{dB}$ and $14.8\,\mathrm{dB}$ in communication and radar mode respectively. The Input compression point ($\mathrm{iP_{1dB}}$) of the receiver is $-28\,\mathrm{dBm}$ and $-20\,\mathrm{dBm}$ in both modes respectively. This way, this multi-mode design addresses the different input linearity requirements of communication and radar functionalities for a JC&S receiver also enabling detection of closer targets. Section II describes the circuit design and implementations detailing the receiver architecture and design of LNA and mixer. Section III covers the measurement results and comparison with state-of-the-art direct-conversion receivers.

II. Circuit Design and Implementation

A. Receiver architecture

The receiver employs a direct-conversion architecture, which includes a multi-mode LNA, a multi-mode differential Gilbert-cell mixer and a baseband buffer as shown in Fig. 1. Traditional receiver designs incorporate Variable Gain Amplifiers (VGA) to provide gain tunability. In this design the gain variablity is integrated in the LNA which will further reduce the power consumption of the system. The LNA and active mixer work in two different gain and linearity modes, enabling JC&S applications. A constant Local Oscillator (LO) signal is fed to the LO port in communication mode, whereas the transmitted signal from the RF transmitter is fed to the LO port in radar mode.

This work is financed on the basis of the budget passed by the Saxon State Parliament.

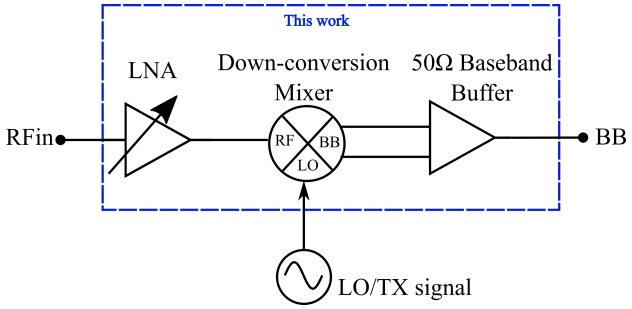

Fig. 1: Receiver architecture with multi-mode LNA, multi-mode mixer and baseband buffer

B. Multi-mode LNA

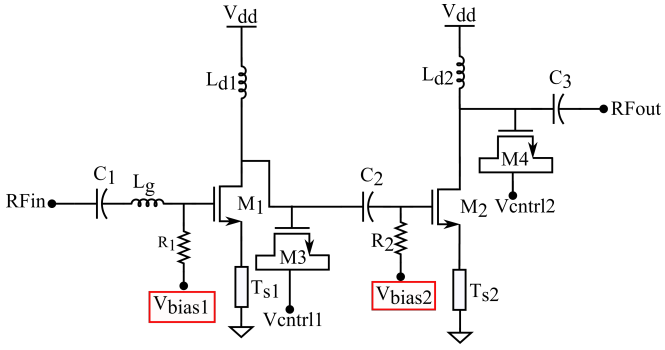

Fig. 2: Circuit diagram of 2-stage common source multi-mode LNA

The schematic view of the multi-mode LNA is shown in Fig. 2. The LNA is realised as a two-stage cascaded common source LNA with source degeneration where the gain variability is made possible by tuning the bias voltages of transistors M1 and M2 using V_{bias1} and V_{bias2}. Foundry library inductors and transmission lines are used as matching elements. The degeneration inductors T_{s1} and T_{s2} are realised using transmission lines with ground shield. The MOS NCAP varactors M3 and M4 in the matching circuits facilitate frequency tuning which can reduce the effect of process variations in the circuit. The biasing of the LNA in both modes is done to keep the devices in saturation region to ensure that the device doesn't introduce non-linearities. The LNA draws a current of $16\,\mathrm{mA}$ and $2\,\mathrm{mA}$ from a $0.8\,\mathrm{V}$ supply in communication and radar modes respectively.

C. Multi-mode Gilbert-cell mixer and baseband buffer

The mixer topology used in this design is a fully differential active Gilbert-cell topology as shown in Fig. 3. The single ended RF output of the LNA and the single ended LO signal are converted into differential input to the mixer RF port and LO port respectively using a baluns before feeding to the mixer core. The mixer core employs the current bleeding technique using resistors R3 and R4 in order to increase the current to the RF transistors M5 and M6. This in turn increases the transconductance of these transistors which increases the conversion gain of the mixer. The multi-mode operation is attained by tuning the bias voltage V_{biasRF} of the RF transistors.

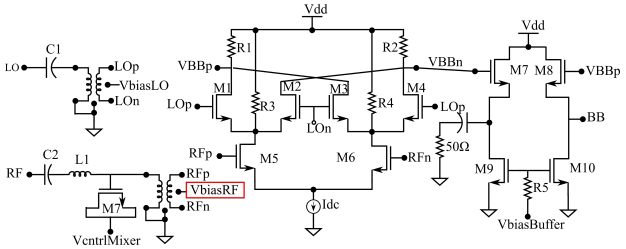

Fig. 3: Circuit diagram of multi-mode Gilbert-cell mixer and baseband buffer

The Gilbert-cell mixer is followed by a source follower buffer. One of the differential baseband output is terminated with a $50\,\Omega$ resistor and the other baseband output is routed to the pad through a $50\,\Omega$ transmission line. The baseband buffer draws a current of $10\,\mathrm{mA}$ and this contributes to the majority of of the power in the mixer block. The baseband buffer also contributes to approximately $2.5\,\mathrm{dB}$ of loss in the system as taken from the simulations. The mixer core itself only draws a current of $6.6\,\mathrm{mA}$ current from a $1.6\,\mathrm{V}$ supply. Since the baseband buffer is implemented in this design only for measurement purposes, the power dissipated in the buffer has been subtracted from the total power consumption of the system. The power in the mixer circuit remain the same in both the modes as the current is set by a constant current source.

III. Simulation and Measurement Results

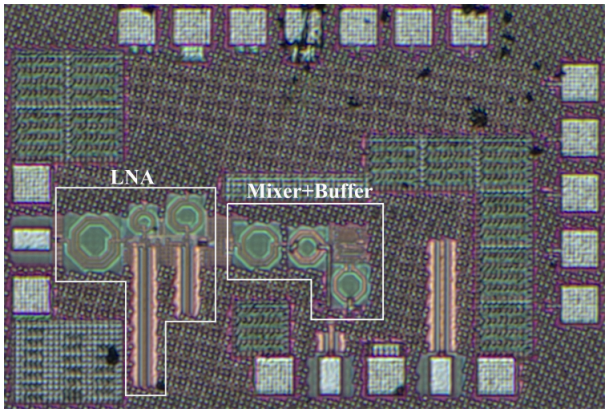

Fig. 4: Micrograph of 25 GHz multi-mode direct conversion receiver with pads

The receiver is fabricated in GlobalFoundries 22nm FDSOI process. It occupies a total area of $0.74\,\mathrm{mm}^2$ with pads and a core area of $0.15\,\mathrm{mm}^2$. The chip micrograph is shown in Fig. 4. The receiver is fully characterized using on-wafer probing. The receiver conversion gain was measured using vector network analyzer (Keysight N5224B) as the input source, signal source (Rohdes & Schwarz SMB100A) as the LO signal and the baseband signal was analysed using the spectrum analyser (Rohdes & Schwarz FSW85). All the measurements were done at an LO power of $5\,\mathrm{dBm}$ directly fed to the LO port of the chip.

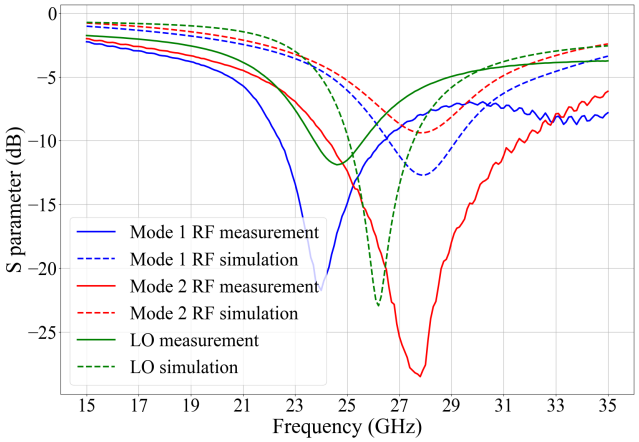

Fig. 5: Measured and simulated S-parameters of the RF port in Communication (Mode1) and Radar (Mode2) modes

The S-parameter measurements of the RF and LO port at the communication and radar modes are shown on Fig. 5. The input reflection coefficient of the LO port doesn't change with the modes of the receiver. The receiver was designed to cover the 5G NR n258 band which is from 24.25 GHz to 27.5 GHz. The measurement results of the RF port in the communication mode and the LO port shows deviation from the simulations and is downshifted in frequency. The radar mode RF S-parameters are in good agreement with the simulations.

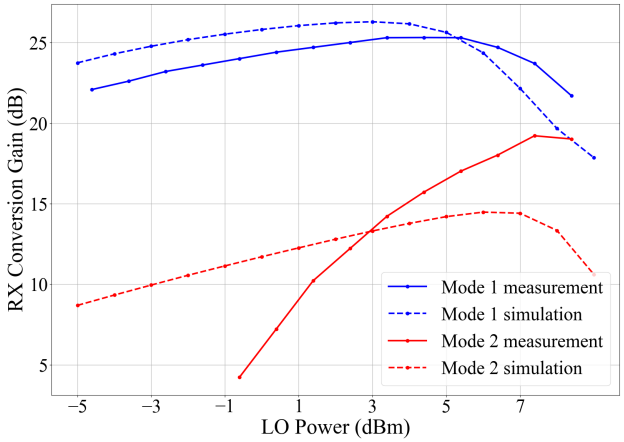

Fig. 6: Receiver output power vs LO power at 25 GHz operating frequency in Communication (Mode1) and Radar (Mode2) modes

Fig. 6 shows the measured and simulated conversion gain values for an LO power sweep with frequency at 25 GHz and an RF signal at 25.1 GHz in communication and radar modes. The LO power was optimized for communication mode. The mixer provides a saturated conversion gain of 24.5 dB in communication mode at an LO power of 5 dB. The measurement data of radar mode shows deviations from the simulations pointing at more non-linearities.

Fig. 7 shows the receiver tuning range which plots the conversion gain across the RF frequency while keeping the

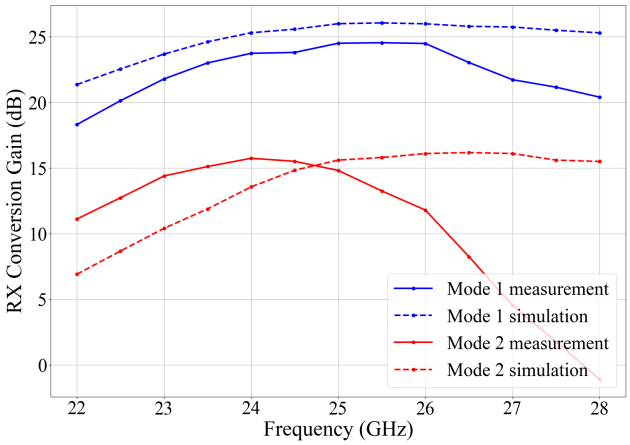

Fig. 7: Receiver conversion gain vs LO frequency at a constant baseband frequency of 100 MHz RF frequency in Communication (Mode1) and Radar (Mode2) modes

baseband frequency constant at 100 MHz. The measurements show that there is a downward shift in the tuning frequency when compared to the simulations. The potential cause can be the presence of additional inductive elements in the design which was not accounted for. Also the highest measured gain is 1.5 dB lower than the measured gain at 25 GHz in communication mode pointing at more losses in the circuit. The receiver in communication mode exhibits a 3-dB bandwidth of 4.3 dB and 3.8 dB in radar mode.

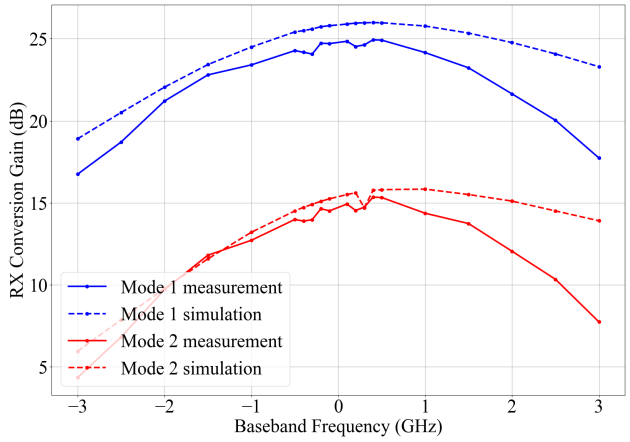

Fig. 8: Receiver conversion gain vs baseband frequency for a fixed RF frequency in Communication (Mode1) and Radar (Mode2) modes

The simulated and measured conversion gain of the receiver for a fixed LO signal at 25 GHz is shown in Fig. 8. The RF signal is swept from 22 GHz to 28 GHz to measure the modulation bandwidth of the receiver. The maximum gain in communication mode is 25 dB and that in the radar mode is 15.3 dB at a baseband frequency of 400 MHz. It is seen that the gain roll-off is much larger when compared to the simulations and the bandwidth of the receiver is much reduced in the measurement results. We attribute the gain roll-off at higher frequencies to the mismatch at LO port at higher

frequencies. It was also observed that the receiver is more sensitive to LO power in the radar mode.

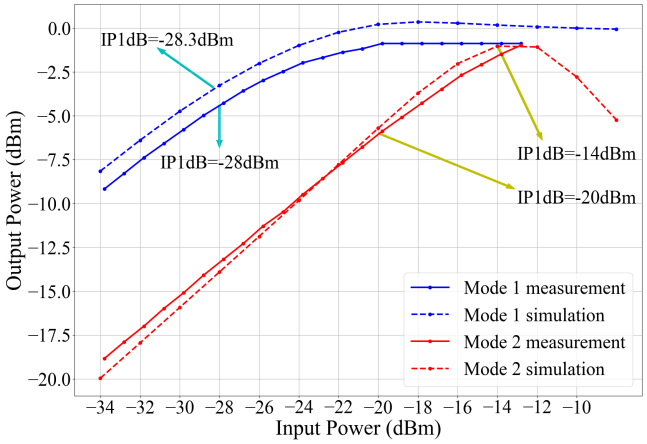

Fig. 9: Receiver output power vs RF input power

The linearity measurements were done by sweeping the RF input power in communication and radar mode at 25 GHz. The linearity plots are depicted in Fig. 9. The measurement and simulated data matches well in communication mode and the measurements show 6 dB degradation in radar mode than in simulations showing more non-linearities in this mode. The receiver exhibits an iP_{1dB} of $-28\,dBm$ and $-20\,dBm$ in communication and radar mode respectively.

The simulated Double Side Band (DSB) noise figure (NF) results at baseband frequency of 1 GHz show a NF of 4.2 dB and 8.2 dB in communication and radar mode respectively.

Table I compares the receiver performance with the state-of-the-art receivers in literature. The proposed receiver compares well with respect to the gain and power consumption. The receiver has the lowest power among other receivers with a comparable gain and iP_{1dB}.

IV. Conclusion

This article presented a 25 GHz multi-mode direct-conversion receiver in 22 nm FDSOI technology for JC&S applications. The gain and linearity tunable receiver provides a peak gain of 24.5 dB and IP1dB of $-28\,dBm$ in communication mode while consuming a DC power of 22.4 mW. The radar mode delivers a maximum receiver gain of 14.8 dB for DC power consumption of 11.63 mW and an iP_{1dB} of $-20\,dBm$. The varactors in the design provide frequency tunability in the RF port which can help the matching in case of process variations. The primary contribution of this article is to demonstrate a multi-mode front-end that addresses the different power requirements of communication and radar usable for JC&S applications. This can be extended with I-Q demodulation techniques for further applications.

TABLE I: Comparison of this work to recent mm-wave receiver designs

	This work	[4]	[5]	[6]	[7]	[8]
Tech	22nm FDSOI	65nm CMOS	45nm SOI	45nm SOI	65nm CMOS	65nm CMOS
Supply (V)	0.8,1.6	-	1.1	1.1	-	-
I-Q demodulation	no	yes	yes	yes	yes	yes
Mutli-mode	yes	no	yes	no	yes	no
3-dB Bandwidth (GHz)	23-27.3	26.75-29.25	24.5-43.5	4-31	38.5-40	9-31
Conv. Gain (dB)	24.5^h 14.8^l	44	35.2^h 18^l	25 @24 GHz	25	43.5 @24GHz
iP_{1dB} (dBm)	-28^h -20^l	-29	-25.5 -7	-17	-15	-
P_{dc} (mW)	22.4^h 11.63^l	98.75	60	$91^{\#}$	531	73
Area (mm^2)	0.15*	1.05	0.52*	1.95	4.65	-

h-max gain, l-min gain, *core area, #RX core

References

[1] C. De Lima et al., "Convergent Communication, Sensing and Localization in 6G Systems: An Overview of Technologies, Opportunities and Challenges," in IEEE Access, vol. 9, pp. 26902-26925, 2021, doi: 10.1109/ACCESS.2021.3053486.

[2] P. Sen et al.,"Joint Communication and Radar Sensing: RF Hardware Opportunities and Challenges—A Circuits and Systems Perspective." Sensors 23.18 (2023): 7673.

[3] M. Sadegh Dadash, S. Bonen, U. Alakusu, D. Harame and S. P. Voinigescu, "DC-170 GHz Characterization of 22nm FDSOI Technology for Radar Sensor Applications," 2018 13th European Microwave Integrated Circuits Conference (EuMIC), Madrid, Spain, 2018, pp. 158-161, doi: 10.23919/EuMIC.2018.8539934.

[4] S. Mondal, L. R. Carley and J. Paramesh, "4.4 A 28/37GHz Scalable, Reconfigurable Multi-Layer Hybrid/Digital MIMO Transceiver for TDD/FDD and Full-Duplex Communication," 2020 IEEE International Solid- State Circuits Conference - (ISSCC), San Francisco, CA, USA, 2020, pp. 82-84, doi: 10.1109/ISSCC19947.2020.9063167.

[5] M. -Y. Huang, T. Chi, S. Li, T. -Y. Huang and H. Wang, "A 24.5–43.5-GHz Ultra-Compact CMOS Receiver Front End With Calibration-Free Instantaneous Full-Band Image Rejection for Multiband 5G Massive MIMO," in IEEE Journal of Solid-State Circuits, vol. 55, no. 5, pp. 1177-1186, May 2020, doi: 10.1109/JSSC.2019.2959495.

[6] J. Dean, S. Hari, A. Bhat and B. A. Floyd, "A 4-31GHz Direct-Conversion Receiver Employing Frequency-Translated Feedback," ESSCIRC 2021 - IEEE 47th European Solid State Circuits Conference (ESSCIRC), Grenoble, France, 2021, pp. 187-190, doi: 10.1109/ESSCIRC53450.2021.9567779.

[7] Y. -S. Ng et al., "A 38-GHz Millimeter Wave Transmission System for Unmanned Aerial Vehicle in 65 nm CMOS," 2022 17th European Microwave Integrated Circuits Conference (EuMIC), Milan, Italy, 2022, pp. 181-184, doi: 10.23919/EuMIC54520.2022.9923486.

[8] Z. G. Boynton and A. Molnar, "RTu1B-3 A 9-31GHz 65nm CMOS Down-Converter with ¿4dBm OOB B1dB," 2020 IEEE Radio Frequency Integrated Circuits Symposium (RFIC), Los Angeles, CA, USA, 2020, pp. 279-282, doi: 10.1109/RFIC49505.2020.9218432.